UCLA

UCLA Previously Published Works

Title

pH-weighted molecular MRI in human traumatic brain injury (TBI) using amine proton chemical exchange saturation transfer echoplanar imaging (CEST EPI)

Permalink

https://escholarship.org/uc/item/46q7d75v

Authors

Ellingson, Benjamin M
Yao, Jingwen
Raymond, Catalina
et al.

Publication Date

2019

DOI

10.1016/j.nicl.2019.101736

Peer reviewed

pH-weighted molecular MRI in human traumatic brain injury (TBI) using amine proton chemical exchange saturation transfer echoplanar imaging (CEST EPI)

Benjamin M. Ellingson[a,d,*], Jingwen Yao[a,c], Catalina Raymond[a,b], Ararat Chakhoyan[a,b], Kasra Khatibi[e], Noriko Salamon[b], J. Pablo Villablanca[b], Ina Wanner[e], Courtney R. Real[e], Azim Laiwalla[e], David L. McArthur[e], Martin M. Monti[d,e], David A. Hovda[e], Paul M. Vespa[e]

[a] UCLA Center for Computer Vision and Imaging Biomarkers, David Geffen School of Medicine, University of California Los Angeles, Los Angeles, CA, USA
[b] Dept. of Radiological Sciences, David Geffen School of Medicine, University of California Los Angeles, Los Angeles, CA, USA
[c] Dept. of Bioengineering, Henry Samueli School of Engineering and Applied Science, University of California Los Angeles, Los Angeles, CA, USA
[d] Dept. of Psychiatry and Biobehavioral Sciences, David Geffen School of Medicine, University of California Los Angeles, Los Angeles, CA, USA
[e] Dept. of Neurosurgery, UCLA Brain Injury Research Center, David Geffen School of Medicine, University of California Los Angeles, Los Angeles, CA, USA

ARTICLE INFO

ABSTRACT

Cerebral acidosis is a consequence of secondary injury mechanisms following traumatic brain injury (TBI), including excitotoxicity and ischemia, with potentially significant clinical implications. However, there remains an unmet clinical need for technology for non-invasive, high resolution pH imaging of human TBI for studying metabolic changes following injury. The current study examined 17 patients with TBI and 20 healthy controls using amine chemical exchange saturation transfer echoplanar imaging (CEST EPI), a novel pH-weighted molecular MR imaging technique, on a clinical 3T MR scanner. Results showed significantly elevated pH-weighted image contrast (MTR_{asym} at 3 ppm) in areas of T2 hyperintensity or edema (P < 0.0001), and a strong negative correlation with Glasgow Coma Scale (GCS) at the time of the MRI exam ($R^2 = 0.4777$, $P = 0.0021$), Glasgow Outcome Scale - Extended (GOSE) at 6 months from injury ($R^2 = 0.5334$, $P = 0.0107$), and a non-linear correlation with the time from injury to MRI exam ($R^2 = 0.6317$, $P = 0.0004$). This evidence suggests clinical feasibility and potential value of pH-weighted amine CEST EPI as a high-resolution imaging tool for identifying tissue most at risk for long-term damage due to cerebral acidosis.

1. Introduction

Traumatic brain injury (TBI) is a major world health problem (Ghajar, 2000; Maas et al., 2008) and it is one of the leading causes of mortality and disability (Finfer and Cohen, 2001). A cascade of biological events occurs following traumatic insult to the brain leading to long-term secondary brain damage, including tissue ischemia from impaired cerebral perfusion (Coles et al., 2002; Diringer et al., 2002), amino acid excitotoxicity (Faden et al., 1989), and interstitial acidification (Hum and Traystman, 1996; Siesjo et al., 1993) from the resulting energy depletion and metabolic crisis (Vespa et al., 2005). Each of these physiologic changes have been shown to be directly or indirectly related to the degree of neuronal damage following injury and may be useful for predicting outcome. Reduced cerebral perfusion has been shown to be linked with outcome (Kirkness et al., 2005; Prabhakar et al.,

2014), while the degree of excitotoxicity has also been linked with outcome (Timofeev et al., 2011) and is the target of a variety of treatment strategies (Willis et al., 2004). Extracellular acidosis within the brain following TBI occurs due to metabolic dysfunction and results in a variety of subsequent injury mechanisms including increased permeability of calcium acid-sensing ion channels (Yermolaieva et al., 2004), further excitotoxic(McDonald et al., 1998) or oxidative(Ying et al., 1999) injury, reduced glutamate uptake by astrocytes(Swanson et al., 1995), impairment of astrocytes to maintain glucose metabolism(Swanson and Benington, 1996), and blood-brain barrier disruption(Nagy et al., 1985). Further, measures of extracellular pH, which is intimately linked with intracellular pH(Mellergard et al., 1994), has been shown to be a strong marker of metabolic dysfunction and has been linked with increased mortality following TBI (Clausen et al., 2005; Timofeev et al., 2013; Yokota et al., 2000). Despite human and
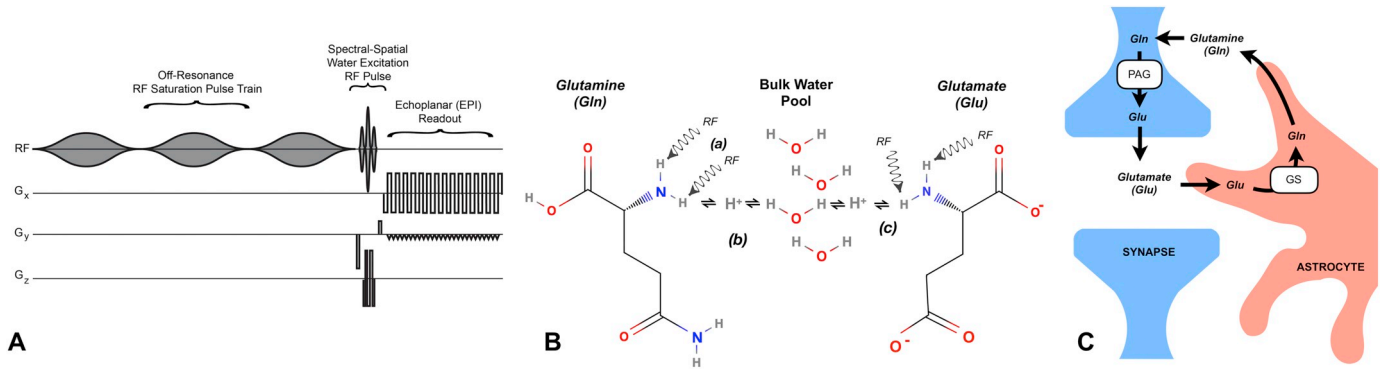
Fig. 1. A) MRI pulse sequence diagram for fast chemical Exchange saturation transfer echo planar imaging (CEST EPI) through one repetition. B) Diagram showing sites of amine proton off-resonance excitation on glutamine (a), which undergoes pH-dependent chemical exchange with the bulk water pool (b). Similarly, glutamate (c) also has exchangeable amine protons, leading to similar CEST effects. C) Diagram showing the glutamine (Gln)-glutamate (Glu) cycle. Glutamate is released from the post-synaptic neuron by either damage to the neuron or normal electrochemical activity. In functioning astrocytes, Glu is transported into the cell where it is converted to Gln via glutamine synthase (GS). Gln within the astrocytes is then shuttled to functioning neurons for Glutamate production by phasphate-activated glutaminase (PAG) or released into the extracellular space in the presence of traumatic insult to either the astrocyte or neuron.

experimental evidence suggesting acidification of the brain may occur after TBI (McIntosh et al., 1987; Shiogai et al., 1999; Zauner et al., 2002), there remains a critical need for tools to non-invasively identifying regions of the brain at risk for low extracellular pH in patients following TBI.

Amine chemical exchange saturation transfer echoplanar imaging (amine CEST EPI; Fig. 1A) is a fast, noninvasive molecular MRI technique with sensitivity to amino acid concentration and pH (Harris et al., 2016; Harris et al., 2018). By preparing the MRI signal through selective saturation of the fast exchanging, pH-dependent amine protons (-NH₂) on glutamine or glutamate (Fig. 1B), amine CEST imaging results in signal contrast in tissues with high glutamine or glutamate concentration *and* low pH. Since there is a well-documented increase in both extracellular glutamate(Bullock et al., 1998; Chamoun et al., 2010; Folkersma et al., 2011; Vespa et al., 1998) and mobile glutamine(Harris et al., 2012; Palmer et al., 1993; Xu et al., 2011) following TBI from damage to neurons and astrocytes (Fig. 1C), respectively, we theorized amine CEST EPI may provide unique insight into the biologic status of the brain independent of other MR image contrasts. We hypothesized areas of T2 hyperintensity adjacent to contusion would exhibit high amine CEST EPI contrast consistent with excitotoxicity and acidification of the brain, which may be useful in subsequent studies to predicting patient outcome by more thoroughly identifying tissue most at risk for long-term damage.

2. Materials and methods

2.1. Theory

The magnetization of water protons undergoing two-compartment chemical exchange with amine protons is described by the Bloch-McConnell equations (Woessner et al., 2005) in the form of:

$$\frac{d\boldsymbol{M}(t)}{dt} = \boldsymbol{X} \cdot \boldsymbol{M}(t) - \boldsymbol{c} \tag{1}$$

where

$$\boldsymbol{M} = \begin{pmatrix} M_{ax} \\ M_{bx} \\ M_{ay} \\ M_{by} \\ M_{az} \\ M_{bz} \end{pmatrix}, \boldsymbol{X} = \begin{pmatrix} C_{2a} & k_b & -\delta a & 0 & 0 & 0 \\ k_a & C_{2b} & 0 & -\delta b & 0 & 0 \\ \delta a & 0 & C_{2a} & k_b & -\omega_1 & 0 \\ 0 & \delta b & k_a & C_{2b} & 0 & -\omega_1 \\ 0 & 0 & \omega_1 & 0 & C_{1a} & k_b \\ 0 & 0 & 0 & \omega_1 & k_a & C_{1b} \end{pmatrix}, \boldsymbol{c} = \begin{pmatrix} 0 \\ 0 \\ 0 \\ 0 \\ M_{az0}/T_{1a} \\ M_{bz0}/T_{1b} \end{pmatrix} \tag{2}$$

pool *a* and pool *b* represent the water and amine protons, respectively; M_{az0} and M_{bz0} are the equilibrium magnetizations of water and amine protons, respectively; k_b is the exchange rate of protons from pool *b* to

pool *a*; k_a is the exchange rate of protons from pool *a* to pool *b* as given by $(M_{b0}/M_{a0}) \cdot k_b$; ω_1 is the RF pulse amplitude as given by $\omega_1 = \gamma B_1(t)$, where γ is the gyromagnetic ratio and $B_1(t)$ is given in μT; $\delta a = \omega - \omega_a$ and $\delta b = \omega - \omega_b$, where ω is the applied radiofrequency (RF) irradiation frequency, ω_a is the water proton resonance frequency, and ω_b is the amine proton resonance frequency; T_{1a} and T_{1b} are the longitudinal relaxation times of water and amine protons, respectively; and $C_{1a} = (1/T_{1a}) + k_a$, $C_{2a} = (1/T_{2a}) + k_a$, $C_{1b} = (1/T_{1b}) + k_b$, $C_{2b} = (1/T_{2b}) + k_b$ represent the sum of exchange and relaxation rates. Eq. 1 can be solved analytically to yield

$$\boldsymbol{M}(t) = e^{\boldsymbol{X}t} \cdot \boldsymbol{M}_0(\boldsymbol{X}/\boldsymbol{c}) - (\boldsymbol{X}/\boldsymbol{c}) \tag{3}$$

The effects of pH on the CEST signal can then be modeled by accounting for the chemical exchange rate between amine and water protons. The chemical exchange between amine and water protons can be characterized as a base-catalyzed process, governed by the equation:

$$k_b = k_0 + k_{base} * 10^{-(14-pH)} \tag{4}$$

where k_0 is the default exchange rate, k_{base} is the base-catalyzed rate constant, and k_b is the exchange rate of protons from the metabolite proton pool to the water pool (Liepinsh and Otting, 1996).

2.2. Phantom preparation and estimation of exchange rate constants

To determine the constants k_0 and k_{base} for amino acid amines, a series of glutamine and glutamate phantoms with pH ranging from 4.8 to 7.5 were prepared for MRI evaluation. Glutamine or glutamate were combined with phosphate-buffered saline (PBS) in 50 mL falcon tubes to reach a concentration of 50 mM. 0.5 mM Gd-DTPA (Magnevist®) was then into each phantom solution to reduce relaxation times (i.e. T_1 and T_2) near physiologic levels. The pH values of sample solutions were then titrated to 18 different values ranging from 4.8 to 7.5, with acid (1 N HCl) and base (1 N NaOH) solution. Phantom pH values were recorded after the MRI scanning and used as the final pH values for data fitting using the Bloch-McConnell equations described previously.

2.3. Mathematical simulations of CEST effects

To demonstrate the relationship between amine CEST image contrast and pH for both glutamine and glutamate we employed the Bloch-McConnell simulation framework for CEST EPI previously described (Harris et al., 2016), using exchange rate values estimated from phantom experiments. Specifically, we simulated the z-spectrum from pH values ranging from 5.5 through 8.0 by first assuming the concentration of amine protons was 50 mM, which is reasonable

considering 1) the concentration of amino acids in normal neural tissues has been estimated around 20–25 mM (Perry et al., 1971); 2) many amino acid derivative metabolites including norepinephrine, 5-hydroxytryptophan, levodopa and other neurotransmitters possess a similar amine functional group that will also contribute to the CEST signal at 3.0 ppm; and 3) we have previously shown these amino acids exhibit similar pH-dependent exchange rate characteristics and CEST effects (Harris et al., 2015). Additionally, we assumed the MR characteristics of water protons were similar to values in normal white matter (T_{1a} = 1.22 s, T_{2a} = 0.107 s) (Harris et al., 2015; Wright et al., 2008), assumed the MR characteristics of the amine protons were similar to those in the literature (T_{1b} = 0.2 s and T_{2b} = 0.1 s) (Choi et al., 2006; Li et al., 2008; Traber et al., 2004; Woessner et al., 2005), and used a set of 3×100 ms Gaussian radiofrequency CEST saturation pulses with an amplitude of 6 μT, similar to previous studies (Harris et al., 2016; Harris et al., 2018). Lastly, using similar values of T_1 and the exchange rates estimated from the phantom experiments, we simulated the CEST signal for a range of concentrations from 5 mM to 50 mM and a range of transverse relaxation times from T_2 = 50 ms to 500 ms.

2.4. Quantification of CEST contrast

During a CEST imaging experiment, the RF saturation frequency ω is swept across a range of values to obtain a "z-spectrum" (Bryant, 1996). To reduce the effects of T_1 and T_2 weighting along with other variables, the attenuation of bulk water magnetization following a saturation pulse is often described by the magnetization transfer ratio (*MTR*), given by:

$$MTR(\omega) = \frac{S(\omega)}{S_0}$$

(5)

where $S(\omega)$ is the magnitude of water proton MR signal available after the saturation pulse with frequency ω and S_0 is the MR signal available without application of any RF saturation pulses. Since *MTR* can be affected by symmetric effects of direct water saturation and conventional magnetization transfer effects, CEST contrast is often described by the asymmetry in the magnetization transfer ratio (*MTR*$_{asym}$) with respect to water proton resonance:

$$MTR_{asym}(\omega) = \frac{S(-\omega) - S(\omega)}{S_0}$$

(6)

For the current simulation, *MTR* at spectral points between -5.0 and $+5.0$ ppm were calculated to obtain simulated z-spectra in these tissues, and the *MTR*$_{asym}$ at 3.0 ppm was used as a final measure of pH-dependent amine CEST contrast for use in subsequent patient studies.

2.5. Human participants

A total of 17 patients with traumatic brain injury and 20 healthy volunteers were enrolled in this prospective, Health Insurance Portability and Accountability Act (HIPAA) compliant study approved by the Institutional Review Board at our institution. All patients and volunteers signed informed written consent to have advanced imaging collected. A summary of TBI patient demographics is shown in Table 1.

2.6. Magnetic resonance imaging

All patients underwent anatomic and amine CEST-EPI on a 3T MR scanner (Siemens Trio, Prisma, or Skyra; Siemens Medical; Erlangen, Germany). All patients received a standardized anatomic imaging protocol consisting of at least T2-weighted turbo spin echo images, diffusion tensor images (DTI), susceptibility-weighted gradient echo images (SWI), fluid-attenuated inversion recovery (FLAIR) images, and 1 mm isotropic parameter matched 3D inversion-recovery gradient recalled echo (IR-GRE) images. Amine CEST-EPI was collected with the following scan parameters: field-of-view (FOV) = 256 × 256 mm,

Table 1
Traumatic Brain Injury (TBI) patient demographics.

| Subject ID	Age/Gender	Injury	Diagnosis	Days from Injury to MRI	ED GCS	GCS @ MRI	6 Month GOSE
1	45M	Fall while Hang Gliding	DAI and WM Microhemorrhages	182	5	10	3
2	35M	MVA with Pedestrian	Bilateral SAH and IPH	3	7	7	3
3	28M	MVA	Bilateral hemorrhagic contusions, SAH in frontal lobe, SDH along cerebral convexities	37	11	3	4
4	37M	Fall from 25 ft. roof	Skull fracture; SDH; L MLS and subfalcine herniation	9	4	6	2
5	20F	MVA with Pedestrian	R SDH; frontal contusions; SAH	1	3	3	3
6	74M	MVA with Pedestrian	SAH; Contusions	8	6	7	–
7	22M	MVA	L temporal hemorrhagic contusion; SAH; SDH	1	8	10	4
8	24M	MVA with Motorcycle	Frontal extraaxial hematomas; midline shift; scattered contusions	9	6	7	7
9	22M	MVA with Bicycle	L Frontal Hemorrhagic Contusion; diffuse microhemorrhages; DAI	18	15	14	8
10	40M	Hit in head and fall	Epidural and SDH with cerebal edema	4	3	14	5
11	49M	Fall from 15 ft	L Frontal SDH; SAH; L temporal and orbitofrontal hemorrhagic contusions	1	14	12	6
12	55M	MVA	Traumatic SAH; bifrontal SDH	20	3	8	–
13	59M	Fall down stairs	R SDH; SAH; hemorragic contusions orbitofrontal and right temporal lobe	8	3	7	–
14	50M	Bicycle accident	Bifrontal contusions, frontal SDH, scattered SAH	2	12	4	–
15	84M	Presumed fall	R frontoparietal and L temporal contusion, SDH and SAH	2	13	7	–
16	33M	High speed motorcycle accident	Multifocal Parenchymal hemorrhagic contusion, SAH, SDH along falx	1	3	3	1
17	50F	MVA with pedestrian	temporal lobe contusion and SDH	4	14	3	–
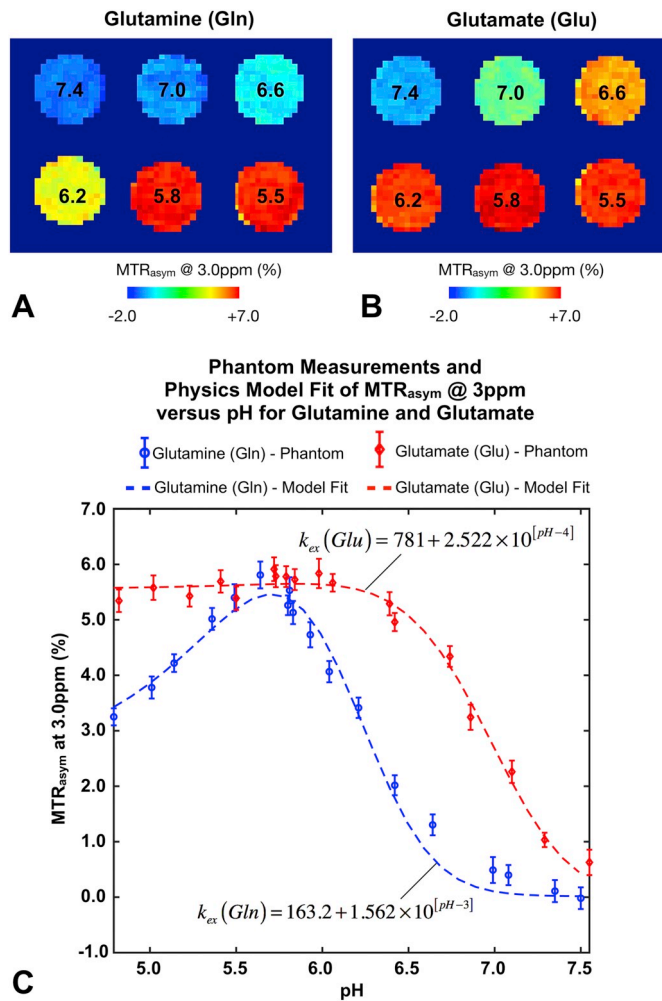
Fig. 2. Amine CEST images of A) glutamine and B) glutamate phantoms with a concentration of 50 mM and varying pH. C) Physical MRI measurements and Bloch-McConnell mathematical model fits for glutamine and glutamate at 5 mM and various pH values used to estimate pH-dependent exchange rates.

matrix size = 128×128, number of slices = 25, slice thickness = 4 mm with no interslice gap, *TE/TR* = 27/380 ms, bandwidth = 1628 Hz, and generalized autocalibrating partially parallel acquisition (GRAPPA) factor = 2. Off-resonance saturation was applied using a pulse train of 3×100 ms Gaussian pulses with amplitude of 6 µT, with spoiling gradients to remove transverse magnetization prior to each readout. A total of 25 off-resonance, or "z-spectral" points were sampled at frequency offsets of: -3.4 to -2.6 ppm, -0.3 to $+0.3$ ppm, and $+2.6$ to $+3.4$ ppm, all in increments of 0.1 ppm. Total scan time for CEST-EPI was approximately 6 min.

2.7. ΔB_0 map estimation using iterative down-sampling estimation with Lorentzian fitting

In order to estimate the static magnetic field distortion, ΔB_0, we employed a novel method using iterative down-sampling with Lorentzian fitting (Yao et al., 2018). Briefly, all CEST data were first preprocessed with motion correction (*mcflirt* function, FSL; Oxford) (Jenkinson et al., 2002). Next, a slice-by-slice ΔB_0 map estimation was achieved by first normalizing the raw CEST data with respect to the S_0 reference scan data, resulting in z-spectral measurements, then performing k-means clustering cluster the pixels with similar patterns in the z-spectrum. The number of clusters for each iteration was set to 3^m, where m is the iteration number. Next, the average z-spectrum data was

estimated across all pixels within the same cluster, and then the mean z-spectrum data were fit to the Lorentzian function in the form: $c - \frac{c}{(x-a)^2 + b}$, where a indicates the shift in z-spectral center point, b relates to the width of the Lorentzian shape, c and b together determine the y-scaling of the function. The constraint bound for ΔB_0 estimation was set to $\pm 1/m$ ppm. The magnetic field distortion, or inhomogeneity in the static magnetic field (ΔB_0), was estimated by the value of a in the Lorentzian model and subsequently stored for all pixels. Lastly, a 3D Gaussian filter with standard deviation of unity was applied to the final ΔB_0 map to remove potential erroneous estimations.

2.8. Region of interest selection

All images were registered to high-resolution, 1 mm isotropic T1-weighted images using a 6° of freedom rigid body transformation and mutual information cost function (FSL, FMRIB, Oxford, UK) for subsequent analyses. MTR_{asym} at 3 ppm and magnetic field fluctuations (ΔB_0) were measured within areas of T2 hyperintensity along with areas of contusion as defined by signal voids on susceptibility (T_2^*) weighted gradient echo images. Additionally, regions with apparent diffusion coefficient (ADC) < 0.6 um^2/ms, suggestive of ischemia, were included. Measurements in patients with multiple sites of T2 hyperintensity, contusion, or potential ischemia were averaged together resulting in a single measurement per patient. As a reference, a 2 cm diameter spherical region of interest was identified within normal-appearing white matter (NAWM), distal from any apparent lesion, hemorrhage or contusion as well as a similar region of interest in white matter within the brains of healthy volunteers. Line plots ranging from 13 to 20 mm were created by traversing the edge of the T2 hyperintense lesion in TBI patients in order to document any apparent spatial colocalization of acidic and ischemic tissue using MTR_{asym} and ADC, respectively.

2.9. Clinical examination and outcome measures

The Glasgow Coma Scale (GCS) is a commonly used clinical measure of initial TBI severity, has been shown to be an early prognostic marker for outcome (Jiang et al., 2002), and is inversely correlated with likelihood of significant morbidity and mortality (Jiang et al., 2002; Lawrence F. Marshall et al., 1991). Average GCS at the time of MRI was 7.4 ± 0.9 S.E.M. (range = 3 to 14). Additionally, we evaluated the extended Glasgow outcome scale (GOSE) at 6 months from the time of injury as a widely accepted clinical measure of outcome in patients with TBI (Jiang et al., 2002; Marshall et al., 1991; Levin et al., 2001; Woischneck and Firsching, 1998). Six-month GOSE scores were available for 11 of the 17 patients in the current study and averaged 4.2 ± 0.6 S.E.M. (range = 1 to 8). In the current study we tested the hypothesis that CEST measures of MTR_{asym} at 3 ppm within T2 hyperintense areas adjacent to contused tissue correlated with GCS at the time of the MRI examination and could predict GOSE 6 months following initial injury.

3. Statistical analyses

All values are presented as mean ± standard error of the mean (S.E.M.). A linear mixed effects model and expected marginal means estimations were used to compare measurements of MTR_{asym} at 3 ppm in regions of normal appearing white matter (NAWM), T2 hyperintense regions, areas of contusion, areas of potential ischemia as indicated by ADC < 0.6 um^2/ms, and healthy white matter from control participants. Similarly, a linear mixed effects model and expected marginal means estimations were used to compare measurements of ΔB_0 at 3 ppm in regions of normal appearing white matter (NAWM), T2 hyperintense regions, areas of contusion, and measurements from white matter in healthy volunteers. A total of 5 comparisons were performed for MTR_{asym} and ΔB_0 at 3 ppm, so a Bonferroni-corrected p-value of
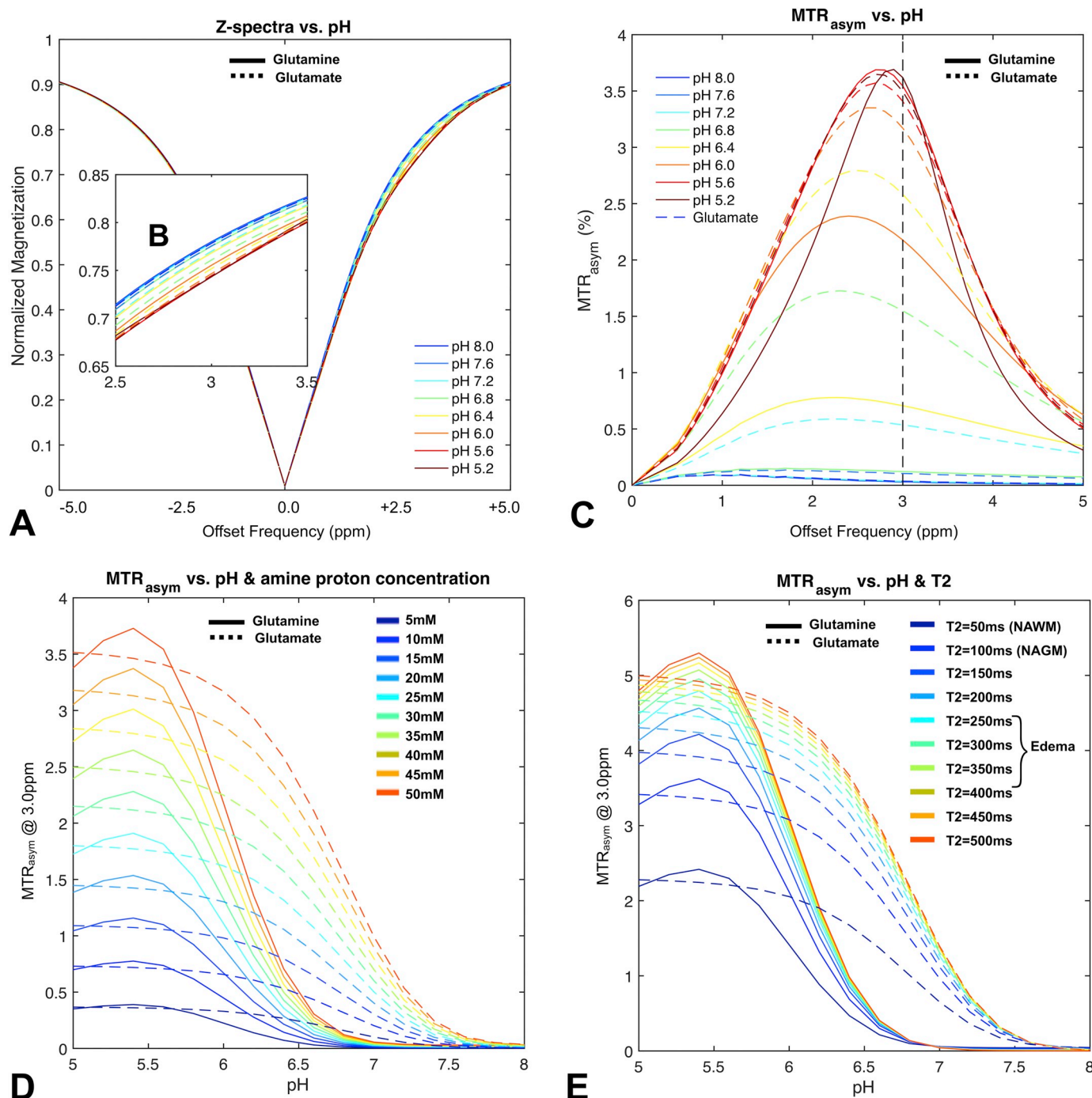
Fig. 3. A) Bloch-McConnell MR simulation results showing *z*-spectra for glutamine and glutamate at 50 mM concentration for various pH. B) Zoomed region of the *z*-spectrum showing increasing attenuation of the MR signal at offset frequencies around +3.0 ppm with decreasing pH. C) Asymmetry in the magnetization transfer ratio about water resonance (MTR$_{asym}$) for glutamine and glutamate at 50 mM and various pH showing maximum asymmetry around +2–3.0 ppm. D) MTR$_{asym}$ at 3.0 ppm for glutamine and glutmate at various concentrations versus pH. E) MTR$_{asym}$ at 3.0 ppm for glutamine and glutamate at 50 mM and various tissue T2 relaxation times versus pH.

0.01 was used to indicate statistical significance. Additionally, linear regression was used to compare CEST measures of MTR$_{asym}$ at 3 ppm within areas of T2 hyperintensity to both GCS at the time of MRI examination and GOSE at 6 months from injury in patients with TBI. We used nonlinear regression to test whether there was a logarithmic association between the time between injury and MRI exam and MTR$_{asym}$ at 3 ppm within areas T2 hyperintensity, which may suggest a higher degree of excitotoxicity and acidosis in the early acute phases of TBI. Lastly, we used a multiple linear regression using a combination of CEST measures and the time between injury and MRI exam in order to

predict both GCS at the time of the MRI exam and GOSE at 6 months from injury.

4. Results

4.1. Phantom and simulation results

Phantom experiments involving CEST imaging of 50 mM vials containing glutamine and glutamate exhibited distinct changes at lower pH values (Fig. 2A–B), consistent with previous studies. Results clearly showed
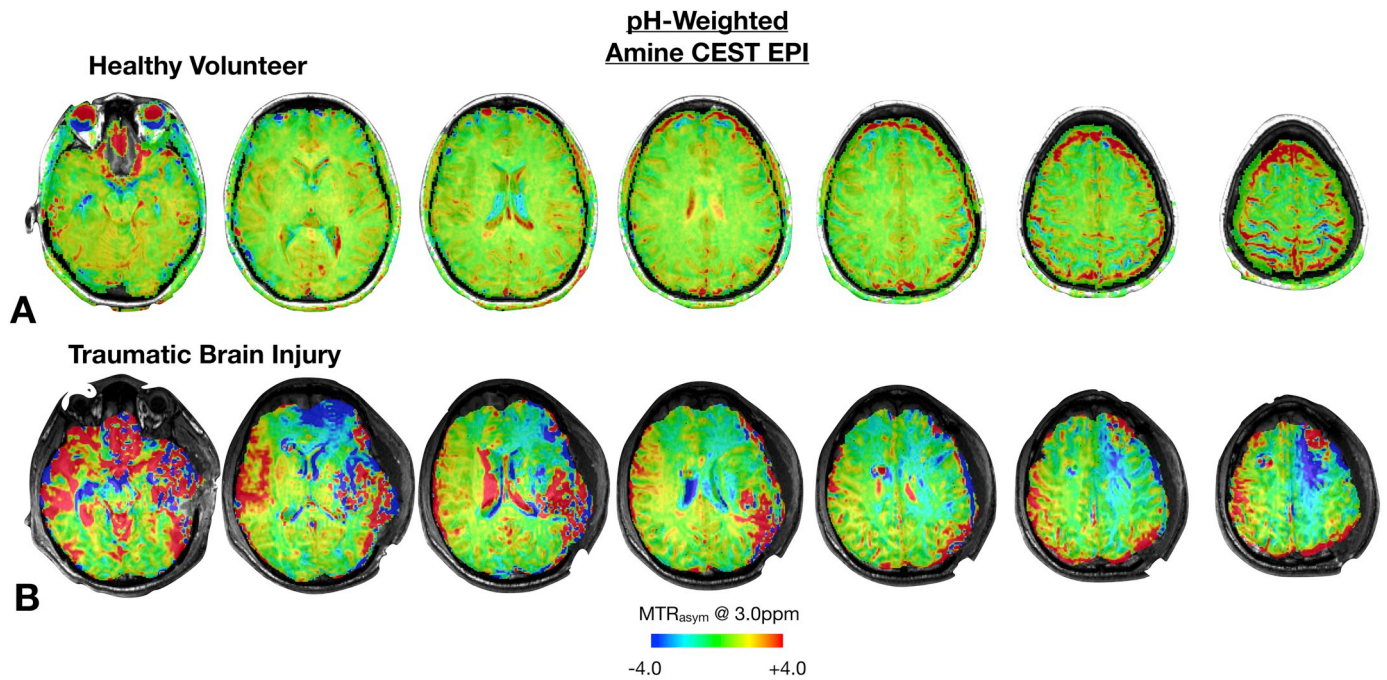
Fig. 4. Example of CEST-EPI estimates of MTR$_{asym}$ at 3 ppm across multiple slices in a A) a 23 year old healthy volunteer and B) a 22 year old patient with TBI (Subject #7).

a higher MTR$_{asym}$ at 3 ppm for pH values below around 7.0 in for glutamine and around 7.5 for glutamate, with an estimated pH-dependent exchange rate, in *Hz*, for glutamine and glutamate of $k_{ex}(Gln) = 163.2 + 1.562 \times 10^{[pH-3]}$ and $k_{ex}(Glu) = 781 + 2.522 \times 10^{[pH-4]}$, respectively (Fig. 2C).

Consistent with previous simulations and other studies (Harris et al., 2016; Harris et al., 2015; Harris et al., 2018; Jin and Kim, 2014; Jin et al., 2012; Sun et al., 2013), CEST measures of MTR$_{asym}$ at 3 ppm from bulk water for both glutamine and glutamate demonstrated sensitivity to pH, concentration, and T2 relaxation time. In particular, the *z*-spectrum showed a slight decrease in normalized MR signal intensity with decreasing pH assuming a constant glutamine concentration of 50 mM (Fig. 3A–B). The MTR$_{asym}$ around 2-3 ppm showed the optimal sensitivity to pH-related amine proton exchange (Fig. 3C), which increased with increasing glutamine and glutamate concentration (Fig. 3D) and increasing tissue T2 (Fig. 3E), which supports the hypothesis that amine CEST EPI may provide value in identifying tissue at risk of acidity due to excitotoxicity, particularly in areas of T2 hyperintensity.

4.2. MTR$_{asym}$ at 3 ppm within NAWM, T2 hyperintensity, contusion and ischemia in TBI

Whole brain CEST-EPI data within healthy volunteers exhibited relatively uniform, low values of MTR$_{asym}$ at 3 ppm (Fig. 4), averaging 0.58% ± 0.05% standard error of the mean (S.E.M.), which was similar to average values of MTR$_{asym}$ at 3 ppm in a 2 cm diameter region of relatively NAWM on anatomic MRI in TBI patients (Fig. 7A; 0.66% ± 0.05%). No difference in MTR$_{asym}$ at 3 ppm was observed between NAWM in TBI patients and white matter in healthy volunteers (*P = 0.2371*). This was in stark contrast to MTR$_{asym}$ at 3 ppm within lesions in TBI patients (Fig. 4). As illustrated in Fig. 5A–C and quantified in Fig. 7A, regions of T2 hyperintensity near areas of contusion exhibited a significantly higher estimate of median MTR$_{asym}$ at 3 ppm (1.62% ± 0.09%) compared with NAWM (Fig. 7A; *P = 0.0007*). Average values of MTR$_{asym}$ at 3 ppm in a 2 cm diameter region of relatively NAWM on anatomic MRI in TBI patients yielded an average value of 0.66% ± 0.05% standard error of the mean (S.E.M.) (Fig. 7A).

In many cases, the acidic lesion appeared larger and more extensive than lesions on anatomic MRI scans (Fig. 6A,B). In the 13 of 17 patients, area of diffuse axonal injury, contusion or hemorrhage on anatomic MRI (as indicated with T$_2$*-weighted SWI) had negative MTR$_{asym}$ at 3 ppm and were easily identifiable on individual patient scans and were often localized within area of the corpus callosum (Fig. 6A–C). Median MTR$_{asym}$ at 3 ppm measured approximately −0.92% ± 0.25%, which was significantly lower than NAWM and the T2 hyperintense lesion (Fig. 7A; *P < 0.0001*). Areas of potential ischemia as indicated by ADC < 0.6 um^2/ms exhibited an average MTR$_{asym}$ at 3 ppm around 0.86% ± 0.34%, which was not significantly different from NAWM (Fig. 7A; *P = 0.4988*). No significant association was observed between ADC and MTR$_{asym}$ at 3 ppm in areas of T2 hyperintensity (Fig. 7B; $R^2 = 0.1267, P = 0.1609$), as also illustrated by the line plots through the T2 hyperintense lesions in Fig. 5A–C, nor between ADC and MTR$_{asym}$ at 3 ppm in areas of contusion (Fig. 7C; $R^2 = 0.1438, P = 0.2013$).

4.3. Magnetic field distortions (ΔB$_0$) within NAWM, pericontusion, and hemorrhage in TBI

Perturbations or distortions in the homogeneous, static magnetic field within the MRI system can lead to errors in MTR$_{asym}$ measurements and may provide unique sensitivity to regions of resolving blood products. The median ΔB$_0$ within NAWM averaged 0.042 ppm ± 0.011 ppm S.E.M., which was not significantly different (*ANOVA, P = 0.1287*) from the ΔB$_0$ estimated within areas of T2 hyperintensity (Fig. 7D; *0.039 ppm ± 0.018 ppm*) or contusion (Fig. 7D; *0.077 ppm ± 0.012 ppm*). No difference was observed between NAWM in TBI patients and white matter from healthy volunteers (*P = 0.8213*), which averaged 0.045 ppm ± 0.009 ppm S.E.M..

4.4. Correlation between MTR$_{asym}$ at 3 ppm and clinical outcome

A strong negative correlation was observed between GCS at the time of MRI and MTR$_{asym}$ at 3 ppm within contusion plus pericontusional tissue (Fig. 8A; $R^2 = 0.4777, P = 0.0021$), suggesting patients with the highest degree of brain acidity had worse function. Similarly, MTR$_{asym}$
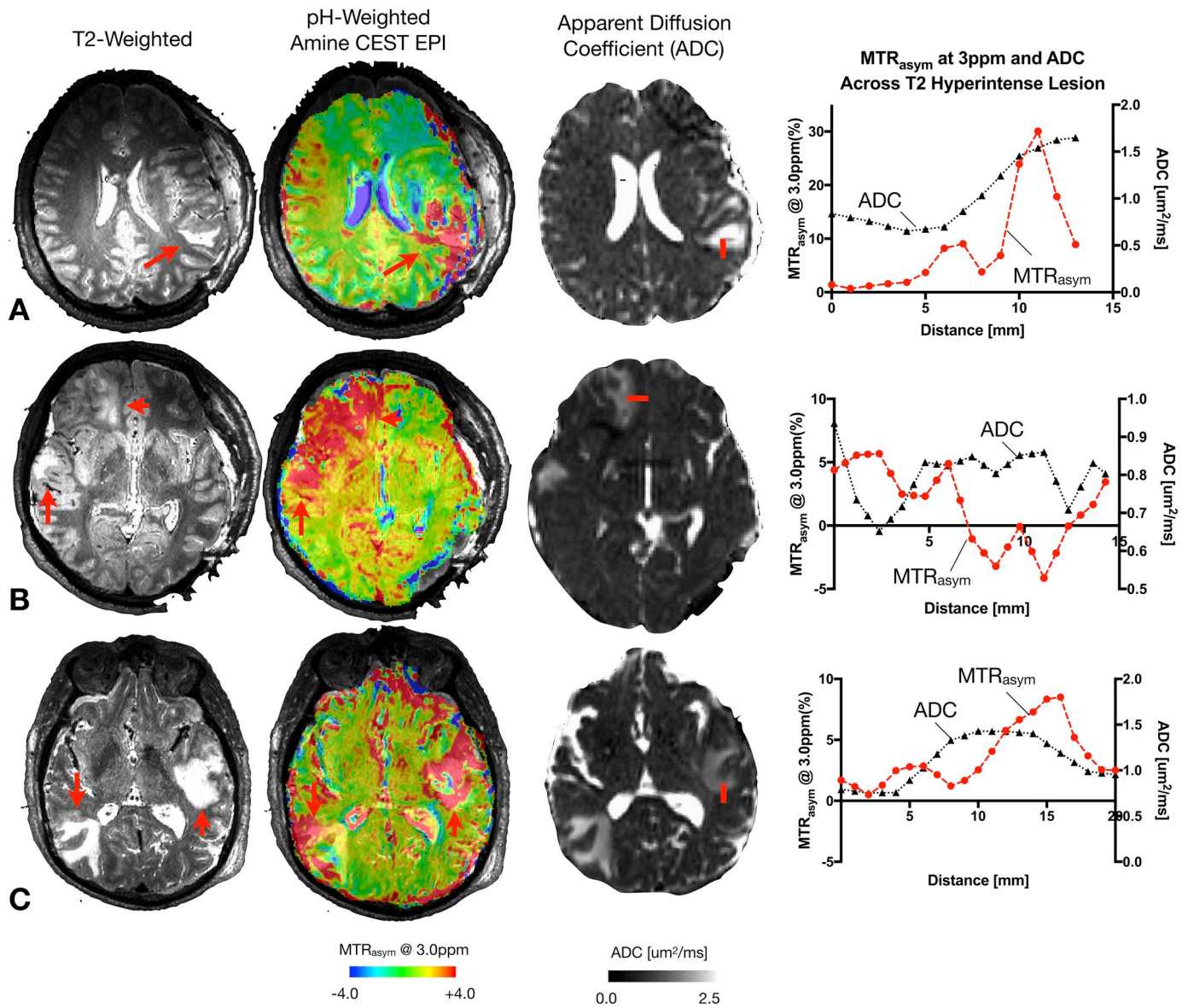
Fig. 5. T_2-weighted anatomic MRI (far left column), pH-weighted amine CEST EPI (MTR_{asym} at 3 ppm, left column), apparent diffusion coefficient (ADC) map (right column), and a line plot showing MTR_{asym} at 3 ppm and ADC through the T2 hyperintense lesion (far right column) in A) a 22 year old male patient (Subject #7) with a left temporal hemorrhagic contusion, subarachnoid hemorrhage, and subdural hematoma following being struck by a motor vehicle; B) a 24 year old male (Subject #8) with a series of frontal extra-axial hematomas, significant midline shift from cerebral edema, and scattered contusions after being hit on a motorcycle by a motor vehicle; and C) a 84 year old male patient (Subject #15) suffered a presumed fall resulting in right frontoparietal and left temporal contusions, subdural hematoma, and subarachnoid hemorrhage. Red arrows on T2-weighted images show sites of T2 hyperintense lesions. Red lines on ADC maps show where line plot measurements were obtained. (For interpretation of the references to color in this figure legend, the reader is referred to the web version of this article.)

at 3 ppm was inversely correlated with GOSE at 6 months (Fig. 8B; $R^2 = 0.5334$, $P = 0.0107$), also suggesting patients with the lowest pH had worse long-term outcomes. We also observed a significant non-linear (logarithmic) association between MTR_{asym} at 3 ppm and the time between the injury and MRI exam (Fig. 8C; *Model: log_{10}(time from injury) = $B \times [MTR_{asym}@3\,ppm] + C$; $R^2 = 0.6317$, $P = 0.0004$*), implying a higher acidity during acute injury compared with more subacute or chronic stages of TBI. Lastly, multiple linear regression suggested a combination of MTR_{asym} at 3 ppm along with the time between injury and MRI could better predict GCS at the time of the MRI exam (Fig. 8D; *Model: GCS = $B_1 \times log_{10}$(time from injury) + $B_2 \times [MTR_{asym}@3\,ppm] + C$; $R^2 = 0.5796$, $P = 0.0004$*) and GOSE at 6 months (Fig. 8E; *Model: GOSE = $B_1 \times log_{10}$(time from injury) + $B_2 \times [MTR_{asym}@3\,ppm] + C$; $R^2 = 0.6539$, $P = 0.0026$*).

5. Discussion

Following TBI, a series of secondary brain damage occurs including reduced cerebral blood flow, hypoxia, and excitotoxicity (Bullock et al., 1995; Bullock et al., 1998; Miller, 1985), all of which result in cerebral acidosis (Clausen et al., 2005; Hovda et al., 1992; Kalimo et al., 1981). Results from the current study are consistent with the hypothesis that areas of T2 hyperintensity adjacent to contusions exhibit significant acidosis, arising from excitotoxicity. Further, our results suggest the degree of acidosis is highly correlated with both clinical function as well as outcome, as evidenced by correlation with GCS at the time of the MRI examination and GOSE at 6 months, respectively. Eloquent studies using multiparametric sensors inserted into the brain in patients with TBI have verified a potential association between low extracellular pH and outcomes including mortality (Gupta et al., 2004; Timofeev
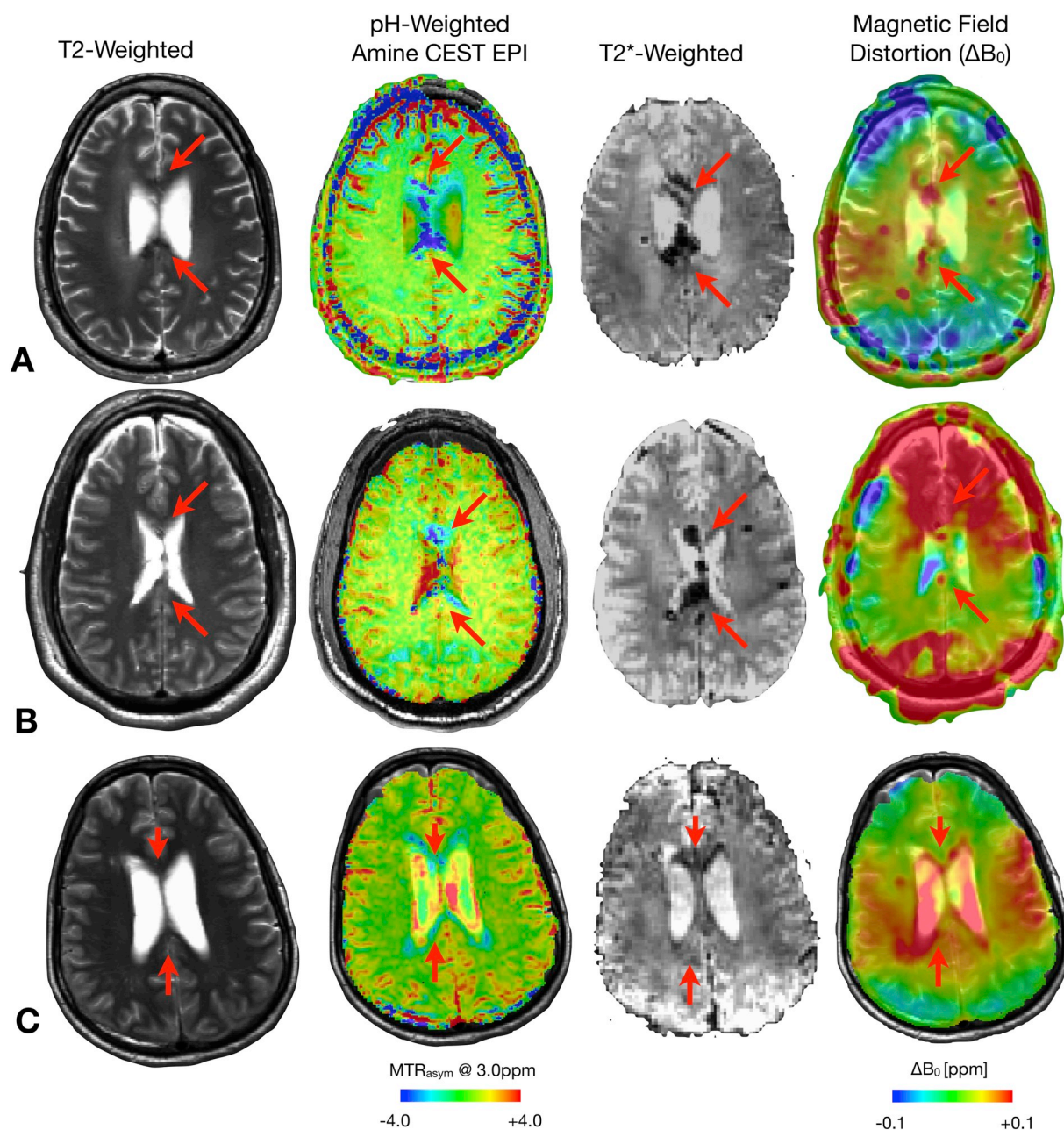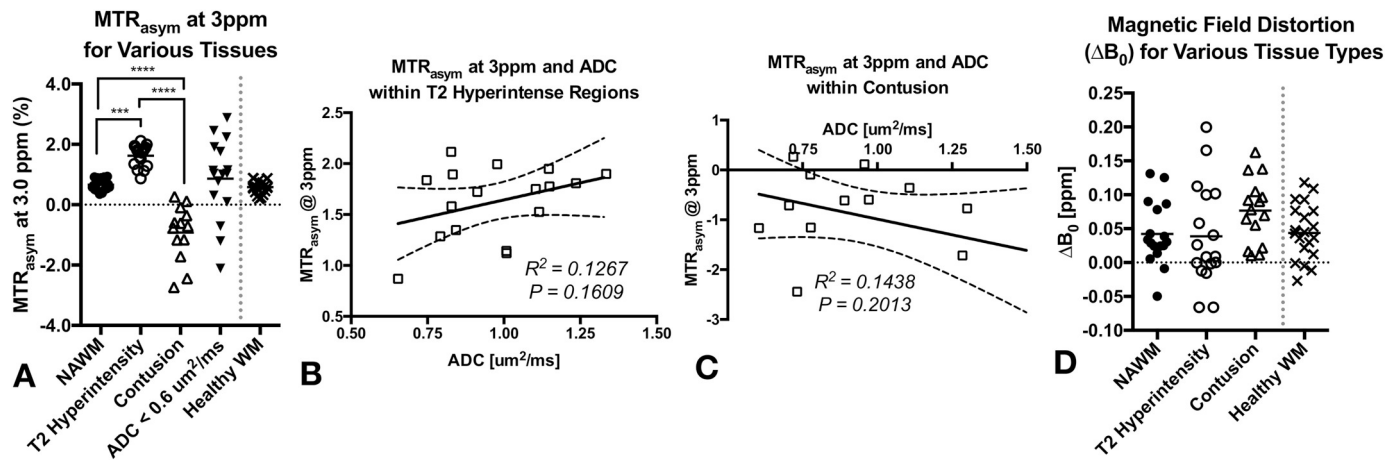
Fig. 7. A) Amine CEST EPI measures of MTR$_{asym}$ at 3 ppm (acidity) in normal appearing white matter (NAWM, solid circles), T$_2$ hyperintense (open circles), regions of contusion T$_2$*-weighted imaging (open triangles), and regions of potential ischemia with ADC < 0.6 um^2/ms. B) Correlation between MTR$_{asym}$ at 3 ppm and ADC within T2 hyperintense lesions. C) Correlation between MTR$_{asym}$ at 3 ppm and ADC in areas of contusion. D) Estimation of magnetic field distortion (ΔB_0) in normal appearing white matter (NAWM, solid circles), T$_2$ hyperintense (open circles), and regions of contusion T$_2$*-weighted imaging (open triangles). *$P < 0.05$; **$P < 0.01$; ***$P < 0.001$; ****$P < 0.0001$.
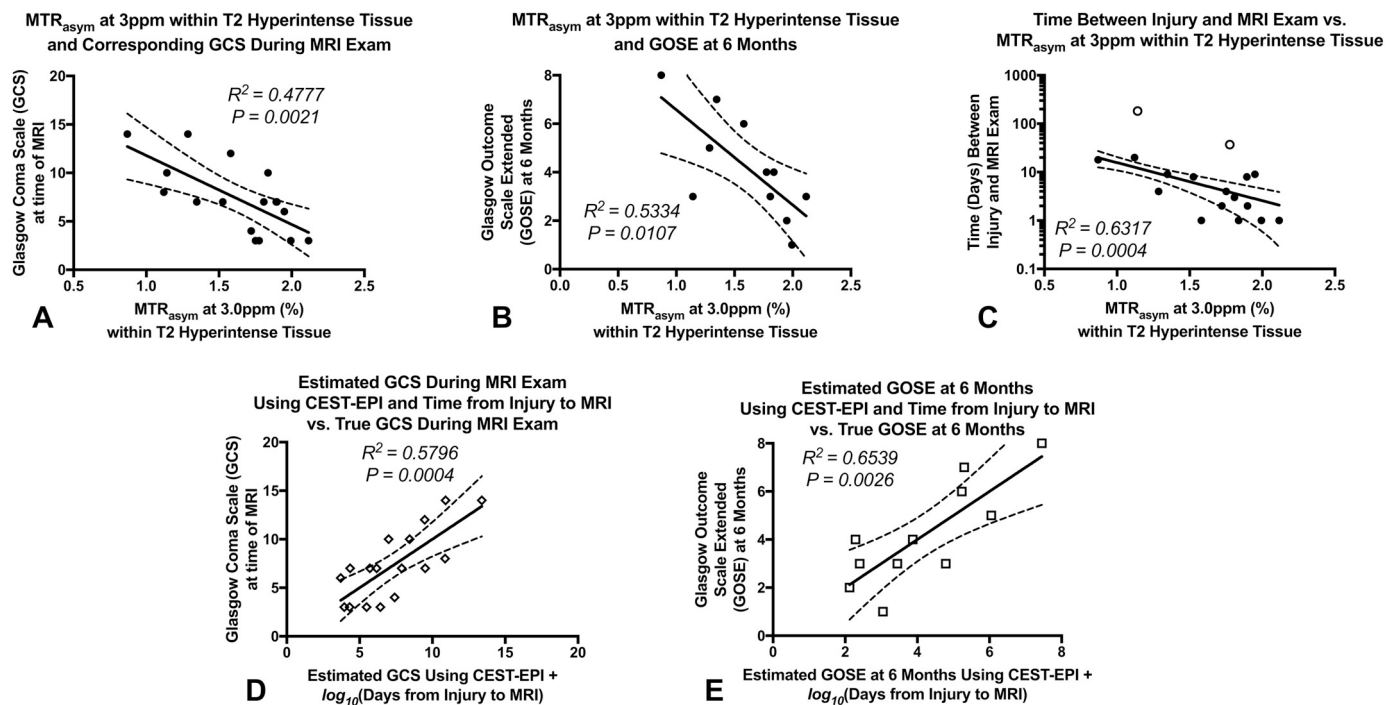

Fig. 8. A) Correlation between MTR$_{asym}$ at 3 ppm within T2 hyperintense regions and Glasgow Coma Scale (GCS) at the time of the MRI exam ($R^2 = 0.4777$, $P = 0.0021$). B) Correlation between MTR$_{asym}$ at 3 ppm within T2 hyperintense regions and the Extended Glasgow Coma Scale (GOSE) at 6 months from the time of injury ($R^2 = 0.5334$, $P = 0.0107$). C) Association between time from injury and MRI exam (log-scale) and MTR$_{asm}$ at 3 ppm within T2 hyperintense regions ($R^2 = 0.6317$, $P = 0.0004$).

EPI can be used to obtain high resolution, whole brain images within clinically realistic scan times.

It is important to point out a few limitations to the current study. First, no correction for B$_1$ inhomogeneities were performed. As B$_1$ can vary as much as ± 20% (Sengupta et al., 2017), our simulations (not shown) suggest that acidic tissue within areas of high amino acid concentration (~50 mM) can have MTR$_{asym}$ at 3 ppm that varies ± 15% (e.g. from 3.65% to 4.3%). Additionally, the results observed in the current study should be taken as preliminary, since the relatively small number of patients included may not represent the strength of trends observed in a larger cohort of patients with different injury profiles. Future studies with a larger number of patients and inclusion of B$_1$ correction are warranted.

In summary, the current study demonstrates the feasibility and potential clinical value of pH-weighted amine CEST EPI as a high-resolution imaging tool for identifying tissue most at risk for long-term damage due to cerebral acidosis. Results suggest low pH in contusion and pericontusional regions correlate strongly with clinical function and 6-month outcome measures.

Author disclosure statement

References

Bryant, R.G., 1996. The dynamics of water-protein interactions. Annu. Rev. Biophys. Biomol. Struct. 25, 29–53.

Bullock, R., Zauner, A., Myseros, J.S., Marmarou, A., Woodward, J.J., Young, H.F., 1995. Evidence for prolonged release of excitatory amino acids in severe human head trauma. Relationship to clinical events. Ann. N. Y. Acad. Sci. 765, 290–297 (discussion 298).

Bullock, R., Zauner, A., Woodward, J.J., Myseros, J., Choi, S.C., Ward, J.D., Marmarou, A., Young, H.F., 1998. Factors affecting excitatory amino acid release following severe human head injury. J. Neurosurg. 89, 507–518.

Chamoun, R., Suki, D., Gopinath, S.P., Goodman, J.C., Robertson, C., 2010. Role of extracellular glutamate measured by cerebral microdialysis in severe traumatic brain injury. J. Neurosurg. 113, 564–570.

Choi, C., Coupland, N.J., Bhardwaj, P.P., Kalra, S., Casault, C.A., Reid, K., Allen, P.S., 2006. T2 measurement and quantification of glutamate in human brain in vivo. Magn. Reson. Med. 56, 971–977.

Clausen, T., Khaldi, A., Zauner, A., Reinert, M., Doppenberg, E., Menzel, M., Soukup, J., Alves, O.L., Bullock, M.R., 2005. Cerebral acid-base homeostasis after severe traumatic brain injury. J. Neurosurg. 103, 597–607.

Coles, J.P., Minhas, P.S., Fryer, T.D., Smielewski, P., Aigbirihio, F., Donovan, T., Downey, S.P., Williams, G., Chatfield, D., Matthews, J.C., Gupta, A.K., Carpenter, T.A., Clark, J.C., Pickard, J.D., Menon, D.K., 2002. Effect of hyperventilation on cerebral blood flow in traumatic head injury: clinical relevance and monitoring correlates. Crit. Care Med. 30, 1950–1959.

Diringer, M.N., Videen, T.O., Yundt, K., Zazulia, A.R., Aiyagari, V., Dacey Jr., R.G., Grubb, R.L., Powers, W.J., 2002. Regional cerebrovascular and metabolic effects of hyperventilation after severe traumatic brain injury. J. Neurosurg. 96, 103–108.

Faden, A.I., Demediuk, P., Panter, S.S., Vink, R., 1989. The role of excitatory amino acids and NMDA receptors in traumatic brain injury. Science 244, 798–800.

Finfer, S.R., Cohen, J., 2001. Severe traumatic brain injury. Resuscitation 48, 77–90.

Folkersma, H., Foster Dingley, J.C., van Berckel, B.N., Rozemuller, A., Boellaard, R., Huisman, M.C., Lammertsma, A.A., Vandertop, W.P., Molthoff, C.F., 2011. Increased cerebral (R)-[(11)C]PK11195 uptake and glutamate release in a rat model of traumatic brain injury: a longitudinal pilot study. J. Neuroinflammation 8, 67.

Ghajar, J., 2000. Traumatic brain injury. Lancet 356, 923–929.

Gupta, A.K., Zygun, D.A., Johnston, A.J., Steiner, L.A., Al-Rawi, P.G., Chatfield, D., Shepherd, E., Kirkpatrick, P.J., Hutchinson, P.J., Menon, D.K., 2004. Extracellular brain pH and outcome following severe traumatic brain injury. J. Neurotrauma 21, 678–684.

Harris, J.L., Yeh, H.W., Choi, I.Y., Lee, P., Berman, N.E., Swerdlow, R.H., Craciunas, S.C., Brooks, W.M., 2012. Altered neurochemical profile after traumatic brain injury: (1)H-MRS biomarkers of pathological mechanisms. J. Cereb. Blood Flow Metab. 32, 2122–2134.

Harris, R.J., Cloughesy, T.F., Liau, L.M., Prins, R.M., Antonios, J.P., Li, D., Yong, W.H., Pope, W.B., Lai, A., Nghiemphu, P.L., Ellingson, B.M., 2015. pH-weighted molecular imaging of gliomas using amine chemical exchange saturation transfer MRI. Neuro-Oncology 17, 1514–1524.

Harris, R.J., Cloughesy, T.F., Liau, L.M., Nghiemphu, P.L., Lai, A., Pope, W.B., Ellingson, B.M., 2016. Simulation, phantom validation, and clinical evaluation of fast pH-weighted molecular imaging using amine chemical exchange saturation transfer echo planar imaging (CEST-EPI) in glioma at 3 T. NMR Biomed. 29, 1563–1576.

Harris, R.J., Yao, J., Chakhoyan, A., Raymond, C., Leu, K., Liau, L.M., Nghiemphu, P.L., Lai, A., Salamon, N., Pope, W.B., Cloughesy, T.F., Ellingson, B.M., 2018. Simultaneous pH-sensitive and oxygen-sensitive MRI of human gliomas at 3 T using multi-echo amine proton chemical exchange saturation transfer spin-and-gradient echo echo-planar imaging (CEST-SAGE-EPI). Magn. Reson. Med. 80, 1962–1978.

Hovda, D.A., Becker, D.P., Katayama, Y., 1992. Secondary injury and acidosis. J. Neurotrauma 9 (Suppl. 1), S47–S60.

Hum, P.D., Traystman, R.J., 1996. pH-associated brain injury in cerebral ischemia and circulatory arrest. J. Intensive Care Med. 11, 205–218.

Jenkinson, M., Bannister, P., Brady, M., Smith, S., 2002. Improved optimization for the robust and accurate linear registration and motion correction of brain images. Neuroimage 17, 825–841.

Jiang, J.-Y., Gao, G.-Y., Li, W.-P., Yu, M.-K., Zhu, C., 2002. Early indicators of prognosis in 846 cases of severe traumatic brain injury. J. Neurotrauma 19, 869–874.

Jin, T., Kim, S.G., 2014. Advantages of chemical exchange-sensitive spin-lock (CESL) over chemical exchange saturation transfer (CEST) for hydroxyl- and amine-water proton exchange studies. NMR Biomed. 27, 1313–1324.

Jin, T., Wang, P., Zong, X., Kim, S.G., 2012. Magnetic resonance imaging of the Amine-Proton EXchange (APEX) dependent contrast. Neuroimage 59, 1218–1227.

Jones, C.K., Huang, A., Xu, J., Edden, R.A., Schar, M., Hua, J., Oskolkov, N., Zaca, D., Zhou, J., McMahon, M.T., Pillai, J.J., van Zijl, P.C., 2013. Nuclear Overhauser enhancement (NOE) imaging in the human brain at 7T. Neuroimage 77, 114–124.

Kalimo, H., Rehncrona, S., Soderfeldt, B., Olsson, Y., Siesjo, B.K., 1981. Brain lactic acidosis and ischemic cell damage: 2. Histopathology. J. Cereb. Blood Flow Metab. 1, 313–327.

Kirkness, C.J., Burr, R.L., Cain, K.C., Newell, D.W., Mitchell, P.H., 2005. Relationship of cerebral perfusion pressure levels to outcome in traumatic brain injury. Acta Neurochir. Suppl. 95, 13–16.

Levin, H.S., Boake, C., Song, J., McCauley, S., Contant, C., Diaz-Marchan, P., Brundage, S., Goodman, H., Kotrla, K.J., 2001. Validity and sensitivity to change of the extended Glasgow Outcome Scale in mild to moderate traumatic brain injury. J. Neurotrauma 18, 575–584.

Li, Y., Srinivasan, R., Ratiney, H., Lu, Y., Chang, S.M., Nelson, S.J., 2008. Comparison of T(1) and T(2) metabolite relaxation times in glioma and normal brain at 3T. J. Magn. Reson. Imaging 28, 342–350.

Liepinsh, E., Otting, G., 1996. Proton exchange rates from amino acid side chains–implications for image contrast. Magn. Reson. Med. 35, 30–42.

Maas, A.I., Stocchetti, N., Bullock, R., 2008. Moderate and severe traumatic brain injury in adults. Lancet Neurol. 7, 728–741.

Marshall, Lawrence F., Gautille, Theresa, Klauber, Melville R., Eisenberg, Howard M., Jane, John A., Luerssen, Thomas G., Marmarou, Anthony, Foulkes, Mary A., 1991. The outcome of severe closed head injury. Spec. Suppl. 75, S28–S36.

McDonald, J.W., Bhattacharyya, T., Sensi, S.L., Lobner, D., Ying, H.S., Canzoniero, L.M., Choi, D.W., 1998. Extracellular acidity potentiates AMPA receptor-mediated cortical neuronal death. J. Neurosci. 18, 6290–6299.

McIntosh, T.K., Faden, A.I., Bendall, M.R., Vink, R., 1987. Traumatic brain injury in the rat: alterations in brain lactate and pH as characterized by 1H and 31P nuclear magnetic resonance. J. Neurochem. 49, 1530–1540.

Mellergard, P., Ouyang, Y.B., Siesjo, B.K., 1994. The regulation of intracellular pH is strongly dependent on extracellular pH in cultured rat astrocytes and neurons. Acta Neurochir. Suppl. (Wien) 60, 34–37.

Miller, J.D., 1985. Head injury and brain ischaemia–implications for therapy. Br. J. Anaesth. 57, 120–130.

Nagy, Z., Szabo, M., Huttner, I., 1985. Blood-brain barrier impairment by low pH buffer perfusion via the internal carotid artery in rat. Acta Neuropathol. 68, 160–163.

Palmer, A.M., Marion, D.W., Botscheller, M.L., Swedlow, P.E., Styren, S.D., DeKosky, S.T., 1993. Traumatic brain injury-induced excitotoxicity assessed in a controlled cortical impact model. J. Neurochem. 61, 2015–2024.

Perry, T.L., Hansen, S., Berry, K., Mok, C., Lesk, D., 1971. Free amino acids and related compounds in biopsies of human brain. J. Neurochem. 18, 521–528.

Prabhakar, H., Sandhu, K., Bhagat, H., Durga, P., Chawla, R., 2014. Current concepts of optimal cerebral perfusion pressure in traumatic brain injury. J. Anaesthesiol. Clin. Pharmacol. 30, 318–327.

Sengupta, A., Gupta, R.K., Singh, A., 2017. Evaluation of B1 inhomogeneity effect on DCE-MRI data analysis of brain tumor patients at 3T. J. Transl. Med. 15, 242.

Shiogai, T., Nara, I., Saruta, K., Hara, M., Saito, I., 1999. Continuous monitoring of cerebrospinal fluid acid-base balance and oxygen metabolism in patients with severe head injury: pathophysiology and treatments for cerebral acidosis and ischemia. Acta Neurochir. Suppl. 75, 49–55.

Siesjo, B.K., Katsura, K., Mellergard, P., Ekholm, A., Lundgren, J., Smith, M.L., 1993. Acidosis-related brain damage. Prog. Brain Res. 96, 23–48.

Sun, P.Z., Lu, J., Wu, Y., Xiao, G., Wu, R., 2013. Evaluation of the dependence of CEST-EPI measurement on repetition time, RF irradiation duty cycle and imaging flip angle for enhanced pH sensitivity. Phys. Med. Biol. 58, N229–240.

Swanson, R.A., Benington, J.H., 1996. Astrocyte glucose metabolism under normal and pathological conditions in vitro. Dev. Neurosci. 18, 515–521.

Swanson, R.A., Farrell, K., Simon, R.P., 1995. Acidosis causes failure of astrocyte glutamate uptake during hypoxia. J. Cereb. Blood Flow Metab. 15, 417–424.

Timofeev, I., Carpenter, K.L., Nortje, J., Al-Rawi, P.G., O'Connell, M.T., Czosnyka, M., Smielewski, P., Pickard, J.D., Menon, D.K., Kirkpatrick, P.J., Gupta, A.K., Hutchinson, P.J., 2011. Cerebral extracellular chemistry and outcome following traumatic brain injury: a microdialysis study of 223 patients. Brain 134, 484–494.

Timofeev, I., Nortje, J., Al-Rawi, P.G., Hutchinson, P.J., Gupta, A.K., 2013. Extracellular brain pH with or without hypoxia is a marker of profound metabolic derangement and increased mortality after traumatic brain injury. J. Cereb. Blood Flow Metab. 33, 422–427.

Traber, F., Block, W., Lamerichs, R., Gieseke, J., Schild, H.H., 2004. 1H metabolite relaxation times at 3.0 tesla: measurements of T1 and T2 values in normal brain and determination of regional differences in transverse relaxation. J. Magn. Reson. Imaging 19, 537–545.

Vespa, P., Prins, M., Ronne-Engstrom, E., Caron, M., Shalmon, E., Hovda, D.A., Martin, N.A., Becker, D.P., 1998. Increase in extracellular glutamate caused by reduced cerebral perfusion pressure and seizures after human traumatic brain injury: a microdialysis study. J. Neurosurg. 89, 971–982.

Vespa, P., Bergsneider, M., Hattori, N., Wu, H.M., Huang, S.C., Martin, N.A., Glenn, T.C., McArthur, D.L., Hovda, D.A., 2005. Metabolic crisis without brain ischemia is

common after traumatic brain injury: a combined microdialysis and positron emission tomography study. J. Cereb. Blood Flow Metab. 25, 763–774.

Vink, R., McIntosh, T.K., Weiner, M.W., Faden, A.I., 1987. Effects of traumatic brain injury on cerebral high-energy phosphates and pH: a 31P magnetic resonance spectroscopy study. J. Cereb. Blood Flow Metab. 7, 563–571.

Wang, W., Zhang, H., Lee, D.H., Yu, J., Cheng, T., Hong, M., Jiang, S., Fan, H., Huang, X., Zhou, J., Wang, J., 2017. Using functional and molecular MRI techniques to detect neuroinflammation and neuroprotection after traumatic brain injury. Brain Behav. Immun. 64, 344–353.

Willis, C., Lybrand, S., Bellamy, N., 2004. Excitatory amino acid inhibitors for traumatic brain injury. Cochrane Database Syst. Rev. 1, CD003986 (Review. PubMed PMID: 14974051).

Woessner, D.E., Zhang, S., Merritt, M.E., Sherry, A.D., 2005. Numerical solution of the Bloch equations provides insights into the optimum design of PARACEST agents for MRI. Magn. Reson. Med. 53, 790–799.

Woischneck, D., Firsching, R., 1998. Efficiency of the Glasgow Outcome Scale (GOS)-Score for the long-term follow-up after severe brain injuries. Acta Neurochir. Suppl. 71, 138–141.

Wright, P.J., Mougin, O.E., Totman, J.J., Peters, A.M., Brookes, M.J., Coxon, R., Morris, P.E., Clemence, M., Francis, S.T., Bowtell, R.W., Gowland, P.A., 2008. Water proton T1 measurements in brain tissue at 7, 3, and 1.5 T using IR-EPI, IR-TSE, and MPRAGE: results and optimization. MAGMA 21, 121–130.

Xu, S., Zhuo, J., Racz, J., Shi, D., Roys, S., Fiskum, G., Gullapalli, R., 2011. Early microstructural and metabolic changes following controlled cortical impact injury in rat: a magnetic resonance imaging and spectroscopy study. J. Neurotrauma 28, 2091–2102.

Yao, J., Ruan, D., Raymond, C., Liau, L.M., Salamon, N., Pope, W.B., Nghiemphu, P.L., Lai, A., Cloughesy, T.F., Ellingson, B.M., 2018 Sep. Improving B(0) correction for pH-weighted Amine Proton Chemical Exchange Saturation Transfer (CEST) imaging by Use of K-means clustering and Lorentzian estimation. Tomography 4 (3), 123–137. https://doi.org/10.18383/j.tom.2018.00017. (PubMed PMID: 30320212; PubMed Central PMCID: PMC6173788).

Yermolaieva, O., Leonard, A.S., Schnizler, M.K., Abboud, F.M., Welsh, M.J., 2004. Extracellular acidosis increases neuronal cell calcium by activating acid-sensing ion channel 1a. Proc. Natl. Acad. Sci. U. S. A. 101, 6752–6757.

Ying, W., Han, S.K., Miller, J.W., Swanson, R.A., 1999. Acidosis potentiates oxidative neuronal death by multiple mechanisms. J. Neurochem. 73, 1549–1556.

Yokota, H., Yamamoto, Y., Naoe, Y., Fuse, A., Sato, H., Unemoto, K., Kurokawa, A., 2000. Measurements of cortical cellular pH by intracranial tonometer in severe head injury. Crit. Care Med. 28, 3275–3280.

Zauner, A., Clausen, T., Alves, O.L., Rice, A., Levasseur, J., Young, H.F., Bullock, R., 2002. Cerebral metabolism after fluid-percussion injury and hypoxia in a feline model. J. Neurosurg. 97, 643–649.